
Gulf of Mexico Gas Hydrate Joint Industry Project Leg II: LWD Methods

Stefan Mrozewski¹, Gilles Guerin¹, Ann Cook¹, Timothy Collett², & Ray Boswell³

Introduction

The downhole logging program during JIP Leg II was designed to assess the distribution and concentration of gas hydrates below the seafloor in the Gulf of Mexico. Six logging-while-drilling (LWD) and measurements-while-drilling (MWD) tools, provided by Schlumberger Drilling & Measurements, were deployed in each hole.

LWD tools are instrumented drill collars in the bottom-hole assembly (BHA), near the bit, that measure *in situ* formation properties. The MWD tool, located in the midst of the LWD tools in the BHA, measures downhole drilling parameters and wellbore direction. The MWD tool also transmits limited LWD data to the surface to be monitored in real-time. Complete LWD data are recorded into downhole computer memory and retrieved when the tools are brought to the surface. The term LWD is often used generically to cover both LWD- and MWD-type measurements, tools and systems.

Powered by batteries or a drilling fluid turbine, LWD tools use non-volatile memory chips to store logging data. The tools take measurements at regular time intervals and are synchronized with an acquisition system on the drilling rig that monitors time and drilling depth. Drilling depth is monitored using a “geolograph” spooled-wire depth encoder attached to the top drive. After drilling, the LWD tools are retrieved and their data downloaded. Synchronization of the uphole and downhole clocks allows merging of the time-depth data (from the surface system) and the downhole time-measurement data (from the tools) into depth-measurement data files. The resulting depth-measurement data are transferred to the Schlumberger Maxwell and IDEAL logging systems for processing.

The LWD tools used during JIP Leg II were the MP3 (multipole acoustic – recently commercialized under the name SonicScope), geoVISION (electrical imaging), EcoScope (propagation resistivity, density and neutron), TeleScope (MWD), PeriScope (directional propagation resistivity), and sonicVISION (monopole acoustic). Because of its slimmer 4.75 inch collar, the MP3 was located behind the 6.75 inch bit and below an 8.50 inch hole-opening reamer, above which were the rest of the 6.75 inch LWD collars. Some tools had stabilizers to centralize the collars in the borehole. Figure [F1](#) shows the configuration of the LWD BHA and Table [T1](#) lists the principal measurements recorded by each tool with the depth of the measurements relative to the bit.

MP3 (SonicScope)

Acoustic measurements while drilling have had to overcome the challenge of insulating propagating acoustic waves from the combined effect of rigid drill collars and the dispersive narrow space between the collars and the borehole wall. Monopole LWD tools – including the sonicVISION tool used during JIP Leg II – record compressional velocity but the strong coupling between the flexural modes of the drill collar and of the borehole prevent LWD dipole sources from recording shear velocity in slow formations (such as the shallow unconsolidated formations targeted in this program). The MP3 uses a quadrupole source to generate a quadrupole mode in the formation, which is entirely decoupled from the drill collar quadrupole mode and can in turn be used to extract the shear velocity of the formation (Kinoshita *et al.*, 2008).

The transmitter of this new tool is a multipole broadband (1-30 kHz) transmitter made of four quadrants that can be excited in phase or in opposition to generate monopole, dipole or quadrupole waves. The receiver section is made

¹Borehole Research Group
Lamont-Doherty Earth Observatory
of Columbia University
Palisades, NY 10964

E-mail:
Cook: acook@ldeo.columbia.edu
Guerin: guerin@ldeo.columbia.edu
Mrozewski: stefan@ldeo.columbia.edu

²US Geological Survey
Denver Federal Center, MS-939
Box 25046
Denver, CO 80225

E-mail:
tcollett@usgs.gov

³National Energy Technology Laboratory
U.S. Department of Energy
P.O. Box 880
Morgantown, WV 26507

E-mail:
ray.boswell@netl.doe.gov

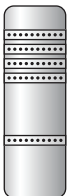









	Collar OD (in)	Max OD (in)	Cumulative Length (ft)	Cumulative Length (m)
 sonicVISION 675 w/ 8-3/8" stabilizer	6.750	8.375	172.60	52.61
 PeriScope 675	6.906	7.500	144.70	44.10
 TeleScope 675	6.890	6.890	123.58	37.67
 EcoScope 675 w/ 8-1/4" stabilizer	6.890	8.250	93.51	28.50
 geoVISION 675 w/ 8-1/4" stabilizer	6.750	8.250	66.85	20.37
 6-3/4" x 8-1/2" hole opener	6.500	8.500	56.81	17.32
 SonicScope 475 (MP3) w/ 2 x 6-1/2" stabilizers	4.750	6.500	51.03	15.55
 Pony drill collar	4.750	4.750	18.37	5.60
 Near-bit stabilizer	4.750	6.500	6.34	1.93
 6-3/4" PDC bit	6.000	6.750	0.86	0.26

Figure F1: Bottom-hole assembly (BHA) used for LWD operations. Collar lengths can be slightly different between versions of individual tools.

Tool	Output	Explanation	Units	Vertical resolution (cm)	Depth of investigation (cm)	Location of sensor from bit (ft)	(m)
sonicVISION		Monopole sonic tool					
	DTCC	Compressional wave slowness	μs/ft	61	~10	163.82	49.93
PeriScope		Directional propagation resistivity					
	AXXH, AXXL, AXXB	Attenuation resistivity at source-receiver spacing XX *	Ω m	55-122	48-102	135.40	41.27
	PXXH, PXXL, PXXB	Phase-shift resistivity at source-receiver spacing XX *	Ω m	21-30	33-79	135.40	41.27
	APWD	Annulus pressure	psi	n/a		131.77	40.16
	GR	Gamma Ray	gAPI			129.74	39.54
TeleScope		MWD, drilling parameters					
	APWD	Annulus pressure	psi			99.63	30.37
EcoScope		Propagation resistivity, density and neutron					
	TNPH	Thermal neutron porosity	%	31		85.57	26.08
	BPHI	Best thermal neutron porosity	%			85.57	26.08
	AXXH, AXXL, AXXB	Attenuation resistivity at source-receiver spacing XX *	Ω m	55-122	48-102	83.74	25.52
	PXXH, PXXL, PXXB	Phase-shift resistivity at source-receiver spacing XX *	Ω m	21-30	33-79	83.74	25.52
	RHOB	Density	g/cm ³	15		77.72	23.69
	APWD	Annulus pressure	psi	n/a		74.30	22.65
	GRMA_FILTER	Calibrated, filtered gamma ray	gAPI	46		73.76	22.48
	DCAV	Density caliper	in				
	IDRO	Image-derived density Oriented density images of borehole wall	g/cm ³				
geoVISION		Resistivity at the Bit Tool					
	GR_RAB_FILTER	Calibrated, filtered gamma ray	gAPI	46		59.45	18.12
	BSAV	Shallow button resistivity average	Ω m	5-8	2.5	62.18	18.95
	BMAV	Medium button resistivity average	Ω m	5-8	8	61.76	18.82
	BDAV	Deep button resistivity average	Ω m	5-8	13	61.18	18.65
	RING	Ring resistivity	Ω m	5-8	18	60.51	18.44
	GR_RAB_FILTER	Calibrated, filtered gamma ray	gAPI	46		59.45	18.12
	RBIT	Bit resistivity	Ω m	30-61	30	57.80	17.62
SonicScope (MP3)		Multipole sonic tool					
	DTCO	Compressional wave slowness	μs/ft			35.45	10.81
	DTSM	Shear wave slowness	μs/ft			35.45	10.81

* Source receiver spacings are XX = 16, 22, 28, 34, 40 in
In the output acronyms: H=2 MHz resistivity; L=400kHz resistivity; B=Blended resistivity

Table T1: Measurement acronyms and units, location of sensors, vertical resolutions and depths of investigation (where available) of the LWD tools used during JIP Leg II. Spacings can be slightly different between versions of individual tools.

of 48 sensors, distributed among four axial arrays that are each aligned with one of the transmitter quadrants. The 4-inch inter-receiver spacing offers the highest resolution of any industry sonic logging tool. The downhole processing capability of the MP3 is also significantly improved from earlier acoustic LWD tools, to enable more complex processing and more reliable real-time evaluation.

Considering the very distinct influence of gas hydrate on the acoustic and elastic properties of marine sediments, the MP3 was added to the JIP Leg II logging string to enable

a more complete characterization of the mechanical properties of the potential hydrate-bearing formations.

The MP3 tool was configured so that waveform data are stored at 10 second intervals, allowing the tool to be on for 160 hours before the downhole memory is filled. The maximum rate of penetration (ROP) to achieve one sample every 6 inches is 180 ft/hr.

geoVISION

The geoVISION resistivity tool (also known as the GVR) provides laterolog-type resistivity measurements of the

formation and high resolution electrical images of the borehole wall. It also contains a scintillation detector that provides an azimuthal gamma ray measurement.

The tool uses two transmitter coils and a number of electrodes to obtain several measurements of resistivity (Bonner *et al.*, 1996):

- **Ring resistivity:** The upper and lower transmitter coils produce currents in the collar that meet at the ring electrode. In a homogeneous medium, these currents flow perpendicular to the tool at the ring electrode. In a heterogeneous formation, this radial current flow is distorted, and the current required through the ring electrode to focus current flow into the formation is related to the formation resistivity. The ring electrode is only 1.5 inches thick and provides a high resolution resistivity measurement.
- **Button resistivity:** The same focusing process used in measuring the ring resistivity is applied to determine the resistivity at three 1-inch button electrodes. Button resistivity measurements made about every 6 degrees as the tool rotates in the borehole are stored and processed to produce a resistivity image of the borehole wall. The deep, medium and shallow button electrodes measure resistivity at three depths of investigation: 5 inches, 3 inches, and 1 inch, respectively and generate resistivity images at each depth of investigation. The tool uses the geomagnetic field to orient the resistivity images to north.
- The geoVISION recorded database density for images is one sample per 1.2 inches. During the JIP Leg II LWD program we used a data acquisition rate of 5 seconds, giving a maximum ROP of 72 ft/hr to produce the highest-resolution images. Under this configuration the geoVISION tool had enough memory to record for more than 14 days.

EcoScope

The EcoScope tool provides a suite of resistivity, geochemical logs, thermal neutron porosity, gamma ray and azimuthal density measurements. The resistivity measurements are propagation resistivities: electromagnetic waves are both attenuated and phase-shifted when they propagate in a formation of finite conductivity, and the degree of

attenuation and phase shift depends on the resistivity of the formation (Bonner *et al.*, 1995; Bonner *et al.*, 1996). Phase-shift resistivity has relatively high vertical resolution and a shallow depth of investigation, while attenuation resistivity has lower vertical resolution and a greater depth of investigation. The dual-frequency (2 MHz and 400 kHz) array of coils in the EcoScope makes 10 phase-shift and 10 attenuation measurements at five transmitter-receiver separations (16, 22, 18, 34, and 40 inches), which correspond to several depths of investigation. For a given frequency, the vertical resolutions of phase-shift resistivities measured at different transmitter-receiver separations are similar. Values for vertical resolution and depth of investigation are listed in Table [T1](#).

For neutron generation the EcoScope uses a pulsed neutron generator (also known as a minitron) and for density logging uses a ^{137}Cs gamma ray source. In addition, the EcoScope provides measurements of elemental capture spectroscopy, neutron gamma density, photoelectric factor, and neutron capture cross-section, or sigma. Drilling optimization measurements include annular pressure while drilling (APWD), ultrasonic and density caliper, and shock detection.

The EcoScope recorded database density for images is one sample per 1.2 inches, and is one sample per 6 inches for all other measurements. During the JIP Leg II LWD program we used an upper data acquisition rate of 4 seconds, giving a maximum ROP of 90 ft/hr to produce the highest-resolution density images. Under this configuration the EcoScope tool had enough memory to record for more than 8 days.

TeleScope

The TeleScope MWD tool transmits data uphole through the fluid in the drill pipe, a process commonly known as “mud-pulse telemetry”. The tool’s modulator generates a continuous 12 Hz pressure wave within the drilling fluid and changes the phase of this signal to transmit relevant bit words representing information from various sensors. Two pressure transducers attached to the standpipe (one near the top and a second near the bottom) on the rig floor acquire the pressure signal which is in turn decoded by the Schlumberger surface software. The MWD real-time data transmission rate is adjustable, depending primarily on water depth and drilling fluid density, and was 6 bits per second during JIP Leg II. Downhole algorithmic data compression further increased the effective data rate.

In addition to the other LWD tools' data, the TeleScope acquires operational and drilling mechanics data including collar RPM, drilling fluid turbine RPM, stick-and-slip, and axial and torsional vibration. The TeleScope also contains a drilling fluid turbine that powers the entire LWD string when drilling fluid is circulated at a sufficient pump rate.

PeriScope

Like the EcoScope, the PeriScope measures propagation resistivity, gamma ray, and has an APWD sensor. The tool's basic resistivity measurements are collected at the same frequencies and have the same vertical resolution and depth penetration as those from the EcoScope.

In addition, the PeriScope contains tilted and transverse coils to obtain directional propagation resistivity, or azimuthal resistivity. JIP Leg II scientists plan to use the azimuthal resistivity measurements to analyze electrical anisotropy associated with gas hydrate-bearing sediments. These advanced analyses are expected to be released in 2010.

The PeriScope recorded database density is one sample per 6 inches. During the JIP Leg II program we used data acquisition rate of 5 seconds, giving a maximum ROP of 360 ft/hr to produce the highest-resolution log curves. Under this configuration the PeriScope tool had enough memory to record for almost seven days.

sonicVISION

The sonicVISION tool records monopole acoustic waveforms in memory and transmits downhole-calculated *P*-wave slowness, as well as the entire slowness time coherence (STC) spectrum, uphole in real-time. Once the tools are returned to the rig floor, recorded waveforms are downloaded and processed to estimate formation *P*-wave slowness and waveform coherence using the Schlumberger Maxwell surface acquisition and processing system.

The principle of the sonicVISION tool is similar to that of wireline array sonic tools (Schlumberger, 1989). The monopole source produces energy around 13 kHz that travels into the formation and refracts back into the borehole. Acoustic waveforms are recorded at four monopole receivers located at 10 ft, 10.67 ft, 11.33 ft, and 12 ft above the source.

Sonic measurements made while drilling are affected by drilling noise. Because the upward propagation of energy in the formation is synchronized with the transmitter firing and any residual drilling noise is not, averaging the waveforms from various consecutive firings increases the relative amplitude of coherent signals. A stack size of approximately eight waveforms is deemed appropriate for these conditions. The sonicVISION tool is kept centralized in the borehole to minimize attenuation of the formation signal in case of asymmetry of the annular space in the hole.

The sonicVISION tool is configured so that waveform data are stored at 10 second intervals, allowing the tool to be on for 256 hours before the downhole memory is filled. The maximum ROP to achieve one sample every 6 inches is 180 ft/hr.

LWD Logging Data Flow and Processing

Data for each LWD logging run were monitored and displayed in real-time using the Schlumberger Maxwell system (supplemented by the Schlumberger IDEAL system for MP3 data). Each time the BHA is brought to the surface, data are downloaded from the tools, processed by Schlumberger to translate acquisition time into depth, and transferred to the shipboard scientists for preliminary interpretation. EcoScope and geoVISION image data were interpreted using Schlumberger's GeoFrame software package.

Gas Monitoring With Real-time LWD Data

Results of previous gas hydrate drilling programs have shown that drilling hazards associated with gas hydrate bearing sections can be managed through careful control of drilling parameters (Birchwood *et al.*, 2007; Collett *et al.*, 2008). However, the possibility of gas flow still exists and the main concern of the LWD monitoring program was to identify free-gas zones that may flow.

The primary measurement used for gas monitoring was annular pressure while drilling, APWD, measured on both the EcoScope and PeriScope tools. The presence of free gas in the borehole lowers the borehole fluid density and decreases the pressure. Sudden pressure increases can also be precursors of gas flow from the formation and into the annulus. The monitoring procedure consisted primarily in observing any abrupt pressure change and being prepared

to control well pressure with drilling fluid if a decrease of 100 psi or more was detected, corresponding to 25% gas saturation in a borehole drilled to 300 mbsf (Aldred *et al.*, 1998).

Interpreting Bedding and Fracture Geometry from geoVISION Images

The orientations of geologic features (including bedding and fractures) were determined from geoVISION electrical resistivity images using Schlumberger’s GeoFrame software. GeoFrame presents geoVISION data as a planar, “unwrapped” 360° resistivity image of the borehole with depth. The image orientation is referenced to north, which is measured by the magnetometers inside the tool, and the hole is assumed to be vertical. Horizontal features appear horizontal on the images, whereas planar, dipping features are sinusoidal in aspect. Sinusoids are interactively fitted to beds and fractures to determine their dip and azimuth. Fractures were identified within geoVISION images by their anomalous resistivity or conductivity and contrasting dip relative to surrounding bedding trends. Differentiating between fractures and bedding planes can be problematic, particularly if both the fractures and bedding have similar dips and orientations.

Gas Hydrate Detection and Evaluation with Downhole Logs

Gas hydrate-bearing intervals are identified by increases in electrical resistivity and acoustic velocities that are not accompanied by a sufficiently corresponding porosity decrease. Gas-bearing intervals can also cause an increase in electrical resistivity, but the presence of gas causes a decrease in the compressional velocity.

Gas hydrates appear light-colored or white on the resistivity images because of their high resistivity contrast with surrounding conductive sediment. A resistivity image is an “unwrapped” 360° image of resistivity in the borehole. The image orientation is referenced to north, as measured by magnetometers inside the tool, and the hole is assumed to be vertical. Horizontal features appear horizontal on the images, whereas dipping features or fractures are sinusoidal.

In Guerin *et al.* (2009a, 2009b, and 2009c), estimates of the gas hydrate saturation, S_h , are calculated using the measured resistivity for Walker Ridge, Green Canyon and Alaminos Canyon JIP Leg II holes. Archie (1942) first

recognized the relationship between the measured resistivity, the porosity, and the amount of oil or gas in the pore space. Archie’s equation is usually used to calculate gas hydrate saturation from resistivity measurements (Pearson *et al.*, 1983; Pearson *et al.*, 1986; Hyndman *et al.*, 1999; Collett and Ladd, 2000; Collett, 2001; Spangenberg, 2001; Malinverno *et al.*, 2008). Often, a modified version of Archie’s equation is used to account for the conductivity effect of clays in clay-rich marine sediments. Erickson and Jarrard (1998) however, showed that shallow, high-porosity marine sediments do not display any conductivity increase due to clay and it is appropriate to apply Archie’s equation:

$$S_h = 1 - \left(\frac{aR_w}{\phi^m R_t} \right)^{1/n} = 1 - \left(\frac{R_o}{R_t} \right)^{1/n} \dots\dots\dots \text{Equation 1}$$

where R_t is the measured RING resistivity, ϕ is porosity, R_w is the resistivity of the pore water and a , m , and n are empirically determined Archie parameters.

Unless otherwise noted, density-derived porosity is used in Equation 1: ϕ is calculated from the IDRO density log, ρ_b , assuming a grain density, ρ_g , of 2.65 g/cc, and a pore water density, ρ_w , of 1.03 g/cc.

$$\phi = \frac{\rho_g - \rho}{\rho_g - \rho_w} \dots\dots\dots \text{Equation 2}$$

Water resistivity (R_w) depends on downhole temperature, pressure, and salinity. Salinity measurements and geothermal gradients were not collected during JIP Leg II. Instead, the geothermal gradient was estimated under the assumption that the bottom-simulating reflector (BSR) on 3-D seismic data was the base of gas hydrate stability. If no BSR was present, the depth was estimated. Several other assumptions were also used to determine the geothermal gradient: a bottom water temperature of 39.2 °F, a salinity of 35 ppt and only methane gas present in the system. The depth of the BSR, the bottom water temperature and the salinity were input into the MMSHYD program developed by the Center for Hydrate Research at Colorado School of Mines to estimate the geothermal gradient. Then, the geothermal gradient, hydrostatic pressure, and salinity were used to calculate R_w using Fofonoff and Millard (1983).

To reduce the unknown parameters in Equation 1, we set the coefficient a to the commonly used value of 1. In terms

of the Archie equation, $a = 1$ is the most realistic value, because $R_t = R_w$ when the porosity is 100%.

To solve for m , intervals are selected from the measured logs from the same hole or site that are 1) water-saturated and 2) similar in lithology or clay content to the target interval of interest. Then, we can solve for m in that interval

$$m = -\frac{\log F}{\log \phi} \quad \text{..... Equation 3}$$

Where F is the formation factor, equal to $R_t = R_w$. Effectively, m is an exponent that modifies the porosity log to match the R_t in water-saturated intervals, and predicts the water-saturated resistivity in hydrate-bearing intervals.

Once the m value is determined, the predicted water-saturated resistivity R_o , is calculated using $R_o = R_w/\phi^m$. In water-saturated intervals, R_o will overlay R_t , and in hydrate bearing intervals R_t will deviate from R_o . Hydrate saturation is calibrated by saturation exponent, n , which depends on the conductivity of the brine in the sediment pore space, sediment grain microstructure, and hydrate saturation history (Spangenberg, 2001). Thus, even the same sediment type may require different values of n . Ranges for n have been determined in the laboratory (Pearson *et al.*, 1983; Spangenberg, 2001; Santamarina and Ruppel, 2008), and *in situ* (Malinverno *et al.*, 2008), however, many of these ranges and values are close to the traditional n exponent, $n = 2$. To show the effect of n within a range that encompasses most of the n values from the published research, gas hydrate saturation in all holes is calculated for $n = 1.5$ and $n = 2.5$.

Density measurements are marginally effected by gas hydrate saturations greater than ~50% (Collett, 1998 and 2001). For gas hydrate saturations above 50%, density porosity was recalculated accounting for the gas hydrate density of 0.91 g/cc, based on the original gas hydrate saturations. Then, a second iteration of gas hydrate saturation was calculated and used for the reports. The second iteration saturations, however, are less than one percent different from the original saturation calculation; even in sediments greater than 90% gas hydrate saturation.

When an m value is difficult to determine, Archie's quick look equation may be applied. This involves directly estimating

the background resistivity R_o , effectively bypassing the calibration of R_w , a and m .

Archie's equation was developed assuming an electrical insulator, like gas hydrate, resides in the primary sediment pore space (Archie, 1942). However, in several occurrences evaluated in JIP Leg II, gas hydrate occurs in secondary pore space in near-vertical fractures and Archie's equation typically overestimates gas hydrate saturation as determined through pressure-core degassing experiments (Lee and Collett, 2009). Lee and Collett (2009) suggest adjusting the Archie parameter m , although this technique requires gas hydrate saturations to be calculated from other methods (such as velocity or pressure cores) to calibrate m .

References

- Aldred, W., *et al.*, 1998. Using downhole annular pressure measurements to improve drilling performance, Oilfield Review, Winter 1998, 40-55.
- Archie, G. E., 1942. The electrical resistivity log as an aid in determining some reservoir characteristics, Transactions AIME, 146.
- Birchwood, *et al.*, 2007. Modeling the mechanical and phase change stability of wellbores drilled in gas hydrates by the Joint Industry Participation Program (JIP) Gas Hydrates Project, Phase II, paper presented at 1997 Annual Technical Conference and Exhibition of the Society of Petroleum Engineers, Anaheim, California, November 11-14, 2007.
- Bonner, S., *et al.*, 1996. Resistivity While Drilling - Images from the String, Oilfield Review, 4-19.
- Bonner, S. D., *et al.*, 1995. New 2-MHz multiarray borehole-compensated resistivity tool developed for MWD in slim holes, in Annu. Tech. Conf. Exhib. Soc. Pet. Eng., edited, Dallas, TX.
- Collett, T. S., 1998. Well log characterization of sediment porosities in gas hydrate-bearing reservoirs, paper presented at 1998 Annual Technical Conference and Exhibition of the Society of Petroleum Engineers, New Orleans, Louisiana, September 27-30, 1998.

- Collett, T. S., and J. Ladd, 2000. Detection of gas hydrate with downhole logs and assessment of gas hydrate concentrations (saturations) and gas volumes on the Blake Ridge with electrical resistivity data, in Proc. ODP Sci. Results, 164, edited by C. K. Paull, *et al.*, pp. 179-191, Ocean Drilling Program, College Station, TX.
- Collett, T. S., 2001. A Review of Well-Log Analysis Techniques Used to Assess Gas-Hydrate-Bearing Reservoirs, in Geophysical Monograph: Natural Gas Hydrates: Occurrence, Distribution and Detection, edited by C. K. Paull and W. P. Dillon, American Geophysical Union, Washington, DC.
- Collett, T.S., Riedel, M., Cochran, J., Boswell, R., Presley, J., Kumar, P., Sathe, A., Sethi, A., Lall, M., Siball, V., and the NGHP Expedition 01 Scientific Party, 2008. Indian National Gas Hydrate Program Expedition 01 Initial Reports: Prepared by the U.S. Geological Survey and Published by the Directorate General of Hydrocarbons, Ministry of Petroleum & Natural Gas (India), 1 DVD.
- Cook, A., Guerin, G., Mrozewski, S., Collett, T.S., Boswell, R., 2009. Gulf of Mexico Gas Hydrate Joint Industry Project Leg II — Walker Ridge 313 LWD Operations and Results: Proceedings of the Drilling and Scientific Results of the 2009 Gulf of Mexico Gas Hydrate Joint Industry Project Leg II. <http://www.netl.doe.gov/technologies/oil-gas/publications/Hydrates/2009Reports/WR313LWDOps.pdf>
- Erickson, S. N., and R. D. Jarrard, 1998. Porosity/formation-factor relationships for high-porosity siliciclastic sediments from Amazon Fan, Geophysical Research Letters, 25(13), 2309-2312.
- Fofonoff, P., and R. C. Millard, 1983. Algorithms for computation of fundamental properties of seawater, UNESCO technical papers in marine science (44), 53.
- Guerin, G., Cook, A., Mrozewski, S., Collett, T. S., Boswell, R., 2009a. Gulf of Mexico Gas Hydrate Joint Industry Project Leg II — Green Canyon 955 LWD Operations and Results: Proceedings of the Drilling and Scientific Results of the 2009 Gulf of Mexico Gas Hydrate Joint Industry Project Leg II. <http://www.netl.doe.gov/technologies/oil-gas/publications/Hydrates/2009Reports/GC955LWDOps.pdf>
- Guerin, G., Cook, A., Mrozewski, S., Collett, T. S., Boswell, R., 2009b. Gulf of Mexico Gas Hydrate Joint Industry Project Leg II — Alaminos Canyon 21 LWD Operations and Results: Proceedings of the Drilling and Scientific Results of the 2009 Gulf of Mexico Gas Hydrate Joint Industry Project Leg II. <http://www.netl.doe.gov/technologies/oil-gas/publications/Hydrates/2009Reports/AC21LWDOps.pdf>
- Hyndman, R. D., *et al.*, 1999. The concentration of deep sea gas hydrates from downhole electrical resistivity logs and laboratory data, Earth and Planetary Science Letters, 172(1-2), 167-177.
- Kinoshita, T., *et al.*, 2008. Next Generation LWD Sonic Tool, paper presented at 14th SPWLA Formation Evaluation Symposium of Japan.
- Lee, M. W. and T. S. Collett, 2009. Gas hydrate saturations estimated from fractured reservoir at Site NGHP-01-10, Krishna-Godavari Basin, India, J. Geophys. Res.114.10.1029/2008jb006237
- Malinverno, A., *et al.*, 2008. Gas hydrate occurrence from pore water chlorinity and downhole logs in a transect across the northern Cascadia margin (Integrated Ocean Drilling Program Expedition 311), Journal of Geophysical Research, 113(B08103).10.1029/2008JB005702
- Pearson, C., *et al.*, 1986. Acoustic and resistivity measurements on rock samples containing tetrahydrofuran hydrates: laboratory analogues to natural gas hydrate deposits, JGR, 91(B14), 14132-14138.
- Pearson, C. F., *et al.*, 1983. Natural-gas hydrate deposits - A review of *in situ* properties, Journal of Physical Chemistry, 87(21), 4180-4185.
- Santamarina, J. C., and C. Ruppel, 2008. The impact of hydrate saturation on the mechanical, electrical, and thermal properties of hydrate bearing sands, silts and clay, in 6th International Conference on Gas Hydrates, edited by P. Englezos, Vancouver, Canada. <https://circle.ubc.ca/handle/2429/2325>

Schlumberger, 1989. Log Interpretation Principles/ Applications, Schlumberger Education Services, Houston, Texas.

Spangenberg, E., 2001. Modeling the influence of gas hydrate content on the electrical properties of porous sediments, Journal of Geophysical Research, 104(B4), 6535-6548.